Wearable Multimodal Vital Sign Monitoring Sensor With Fully Integrated Analog Front End

Yishan Wang, Fen Miao, Qi An, Zengding Liu, Cong Chen, and Ye Li

***Abstract*—Cardiovascular disease (CVD) is a widespread disease and the leading cause of death worldwide. Home care is essential for patients with CVD, and it involves the daily monitoring of important CVD-related vital signs using methods including electrocardiography (ECG), heart rate monitoring, pulse oximetry (SpO2), and continuous blood pressure measurement. However, a wearable device that can monitor these parameters simultaneously remains unavailable; herein, we propose a lightweight, highly integrated sensor that can do so. In this sensor, an analog front end (AFE) integrated chip (IC) is implemented in the sensor to detect one-lead ECG and two-wavelength photoplethysmography (PPG) signals. The highly integrated IC minimizes both the size and power requirement of the sensor. Moreover, its comprehensive functions include adjustable gain, current compensation, lead off, and fast recovery—all of which are crucial for wearable applications in large populations. Accordingly, the sensor can apply the adaptive adjust method to automatically adjust the IC parameters to suit a range of applications and users. In addition, the heart rate is calculated from the R-R interval from the ECG signals, whereas the SpO2 is calibrated with a univariate quadratic equation with less than 1% mean error. Our sensor can also calculate the systolic blood pressure (SBP) and diastolic blood pressure (DBP) by using a support vector machine based calibration-less model with the features of infrared PPG and ECG signals. The model is trained on our pre-collected wearable dataset and has a mean error $\pm$ standard deviation of -2.10 ± 7.07 mmHg for SBP and 0.04 ± 7.34 mmHg for DBP in 16 volunteers. In conclusion, this paper reports on a multimodal, vital sign monitoring sensor—with small size, low power, and dynamic compatibility—suitable for patients with CVD under home care.**

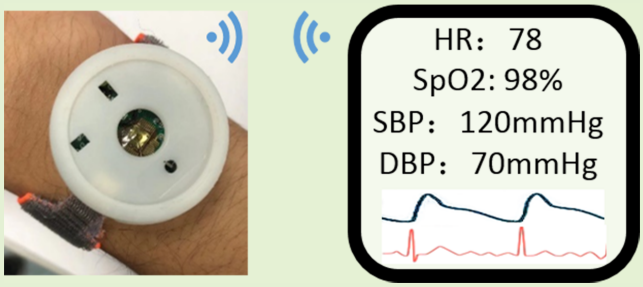

***Index Terms*—Vital sign, multimodal, analog front end, SpO2, blood pressure.**

I. Introduction

THE use of wearable health care devices in various forms such as patches, smart-watches, and wristbands is becoming mainstream [1], [2]. These devices can continuously monitor several physiological signals through various methods such as continuous heart rate (HR) monitoring, pulse oximetry (SpO2), and electrocardiography (ECG) [3], [4]. Thus, devices have key applications in the early diagnosis of diseases such as heart failure and hypertension. However, for more accurate diagnoses, different physiological signals from multisensors must be analyzed in tandem. In other words, for proper diagnosis, several sensors must be worn on the body simultaneously; however, this can inconvenience the user. Recent studies have increasingly focused on the development of multisensor acquisition systems [5]–[7]. For home-care applications, the most suitable wearable device is the smartwatch or wristband. However, currently available smart-watches or wristbands may be able to measure only a few parameters and may need to use multiple modules for detecting different physiological signals, which makes the device bulkier and more complex. A hybrid integrated circuit (IC) could be used as a compact platform for a suite of multisensors. A device with a multisensor IC can detect parameters with minimal size and power requirements [8].

Manuscript received April 19, 2022; accepted May 19, 2022. Date of publication May 23, 2022; date of current version July 1, 2022. This work was supported in part by the National Natural Science Foundation of China under Grant 81901834, in part by the Basic and Applied Basic Research Fund Project of Guangdong Province under Grant 2020A1515010654, in part by the Shenzhen Science and Technology Program under Grant JSGG20201102172002006, and in part by the Shenzhen Application Demonstration Project under Grant KJYY20180703165202011. The associate editor coordinating the review of this article and approving it for publication was Dr. Jurgen Kosel. *(Corresponding author: Ye Li.)*

This work involved human subjects or animals in its research. Approval of all ethical and experimental procedures and protocols was granted by the Institutional Review Board of the Shenzhen Institute of Advanced Technology, Chinese Academy of Sciences, under Approval No. SIAT-IRB-190215-H0287.

The authors are with the Shenzhen Institute of Advanced Technology, Chinese Academy of Sciences, Shenzhen 518055, China (e-mail: ye.li@siat.ac.cn).

Digital Object Identifier 10.1109/JSEN.2022.3177205

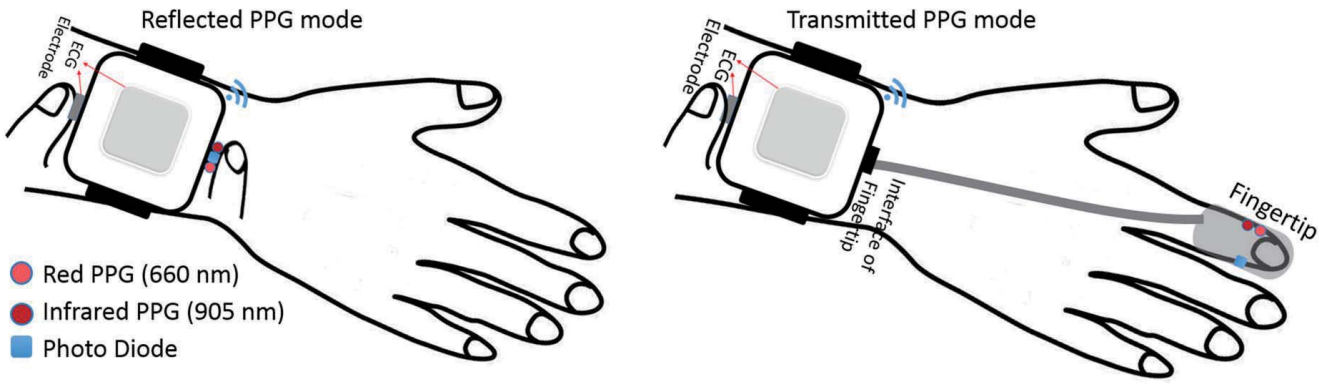

Fig. 1. Overview of the wearable wireless multimodal vital sign–monitoring sensor with reflected and transmitted PPG mode. Both the ECG and PPG signals are detected on the wrist.

Present-day commercial ICs typically can only detect a single parameter. Many studies have investigated the use of system on chip (SoC) technology to detect multiple physiological parameters. The group at imec-Holst Center proposed several multisensor SoCs for health monitoring applications. Another study [9] designed a multisensor acquisition system with ECG, bio-impedance (BIO-Z), galvanic skin response (GSR), and two photoplethysmography (PPG) modules in a readout IC. This readout IC integrates several readout modules for different parameters and consumes approximately 1 mW of power. In another study [10], a reconfigurable analog front end (AFE) IC with a 1.1 mm^2 chip area was presented; to considerably reduce the chip area, the reconfigurable IC structure involved the reuse of the amplifier and filter for different signal readouts. A study [11] proposed a highly integrated SoC that included biosensor readouts, power management circuitry, digital signal processing, and wireless communication (BLE). Two more studies [12], [13] also proposed biosensor SoCs to monitor different signals. However, these studies have focused on chip design but rarely considered application requirements [14]: they did not mention the types of vital signs that could be calculated from the obtained signals or state the specific applications for their chips. Consequently, the application of these chips warrants further evaluation.

In this study, our proposed sensor was designed with practical application in mind. Specifically, we first considered the vital signs that can and must be measured continuously using a wearable sensor. Cardiovascular disease (CVD) is a widespread disease and the leading cause of death worldwide. Most patients with CVD must monitor their vital signs frequently, even at home, to detect anomalies as early as possible. Among these vital signs, electrocardiogram readings, HR, SpO2, and continuous blood pressure are the most crucial. Of these, HR and SpO2 can be calculated from ECG and two-wavelength PPG signals. Cuffless continuous blood pressure measurement can also be performed using ECG and PPG signals [15]–[17]; in our previous works [18]–[20], this technology was confirmed to achieve considerably high accuracy. Hence, we considered the design of an ECG and two-wavelength PPG signal detecting sensor attached to wearable monitor.

Next, we considered the AFE requirements that enable accurate detection of the aforementioned vital sign. In practical applications, the most common biopotential AFE requirements are low power and low noise, followed by adjustable gain (both for ECG and PPG signal detection), a controllable LED driver, ambient current cancellation, detection of the AC and DC components of red and infrared PPG signals (to calculate the SpO2), detection of lead off, and fast recovery function of the ECG channel.

Based on the aforementioned considerations, this paper proposes a multimodal vital sign monitoring sensor. A fully integrated AFE was designed to detect ECG and two-wavelength PPG signals efficiently. In this AFE, the current compensation circuit, adjustable gain, and LED-driven current designed in the PPG channel of AFE allow the sensor to realize adaptive adjustments with high-quality signaling for different users. In the ECG channel, when the leads are reconnected, a lead-off detection and fast recovery circuit was implemented, which shortens the recovery time. In addition, the HR, SpO2, and blood pressure were calculated in real time. The proposed sensor may thus be applicable to home care, providing both practicality and accuracy in different applications and for different users.

II. Design of the Sensor System

As shown in Fig. 1, the proposed sensor, which is worn on the wrist, can detect PPG signals in both reflected and transmitted modes through adaptive adjustment. Moreover, it can detect the ECG and two-wavelength (red and infrared) PPG signals simultaneously. The system contains an AFE IC and an nRF52832, a bluetooth mode including an ARM Cortex M4 microcontroller unit (MCU) and a bluetooth low energy (BLE) transmitter, as shown in Fig. 2. This design provides a fully sensor implementation for extensive wearable applications. It is capable to be used in different modes, but still ensures the high signal quality.

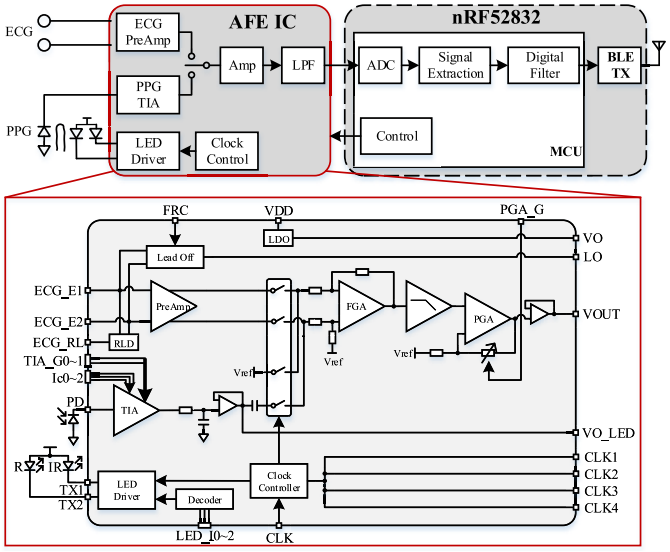

Fig. 2. The architectures of sensor and AFE IC.

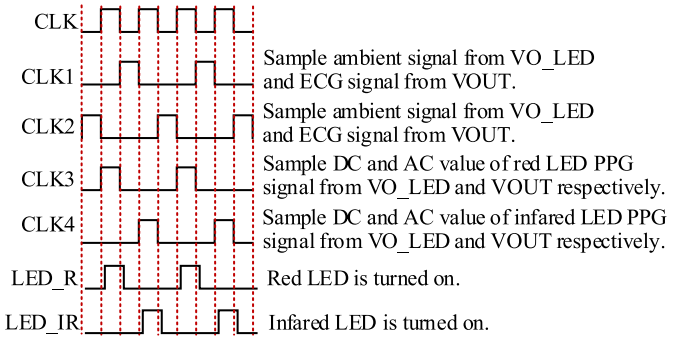

Fig. 3. Clock sequences for ECG and PPG sampling.

TABLE I
CONTROL BITS OF THE LED DRIVER AND CORRESPONDING CURRENTS

Control bit	LED current
000	0 mA
001	7 mA
010	14 mA
011	21 mA
100	28 mA
101	35 mA
110	42 mA
111	49 mA

A. AFE Architecture

To reduce the current consumption of the entire AFE, a reconfigurable structure is applied. This structure includes an ECG channel with a preamplifier and a PPG channel with a transmit impedance amplifier (TIA) that transmits the current from a photodiode (PD) to voltage. It also includes a differential to single ended fixed gain amplifier, a low pass filter and a programmable amplifier (PGA), which are shared by both the ECG and PPG channels. The high-pass filter in ECG channel is provided by the capacitor coupled instrument preamplifier, while in PPG channel, as cutoff frequency is very low, the capacitor of the high-pass filter is applied externally. The operational transconductance amplifier (OTA) of the low-pass filter applies three Gm modules [21], which provides a low cutoff frequency with a small g_m to avoid the need to use a large capacitor. The gain of the PGA is controlled by a setting pin PGA_G. Furthermore, two LEDs are driven by the LED driver.

The clock sequences for ECG and PPG sampling are shown in Fig. 3. The sampling frequency for ECG is twice as big as for PPG. The source clock (CLK) is given by the MCU. Then the AFE IC generates 2 LED clocks (LED_IR and LED_R) to control the LED driver and multiplexer, and 4 sampling clocks (CLK1, CLK2, CLK3, CLK4) to MCU. MCU controls the ADC to sample the different signals by the 4 clocks with the falling edge. CKL1 and CKL2 are used to sample the ambient signal and ECG signal, while CLK3 and CLK4 are used to sample the AC and DC values of red and infrared PPG signals. The LED_IR and LED_R clocks are a little bit delayed from the PPG sampling clocks CLK3 and CLK4, to insure that the LEDs are turned off after the sampling.

The AFE chip architecture is presented in Fig. 2. The details of its main structures are introduced in the subsequent sections.

1) LED Driver: To obtain SpO2 measurements, the AFE driver drives two LEDs (i.e., red and infrared LEDs). The AC amplitude of the PPG signal depends on both the current of the LED and the gain of the TIA. To save power, the current of the LED should be as low as possible. However, low current leads to weak light emission. The current sensed by the PD can be difficult to detect. Furthermore, the thicknesses of fat and other tissues may differ among users. Thus, the LED current must be manipulated according to the application and user conditions.

Here, the current is controlled using three control bits (i.e., LED_I0, LED_I1 and LED_I2) as the inputs of the decoder (Table I). The decoder outputs control eight current sources to supply eight varied LED currents, as shown in Fig. 4(a). The currents of the two LEDs thus can be controlled independently. The current sources (Fig. 4(a)) are optimized between power consumption, output current accuracy, and circuit complexity.

2) TIA With Current Compensation: In the PPG channel, a TIA is designed (Fig. 4(b)). As mentioned, the PPG component amplitude is related to the gain of the TIA. Because lights of different wavelengths transmit to tissues at different depths, both the AC and DC components of the PPG differ for the light of different wavelengths, even with an identical LED-driven current. In addition, different users are expected to have varied PPG component amplitudes. Consequently, the gain of the TIA should be adjustable for different applications and persons.

Herein, this gain is controlled by two control bits (i.e., TIA_G0 and TIA_G1) as the inputs of the decoder. The outputs of the decoder control the switches of the transresistor array, which provides 200 KΩ to 2 MΩ transresistance. The control bits and transresistance values of the TIA are listed in Table II.

The PPG waveform comprises DC and AC components. The DC component results from not only tissues and non-pulsatile

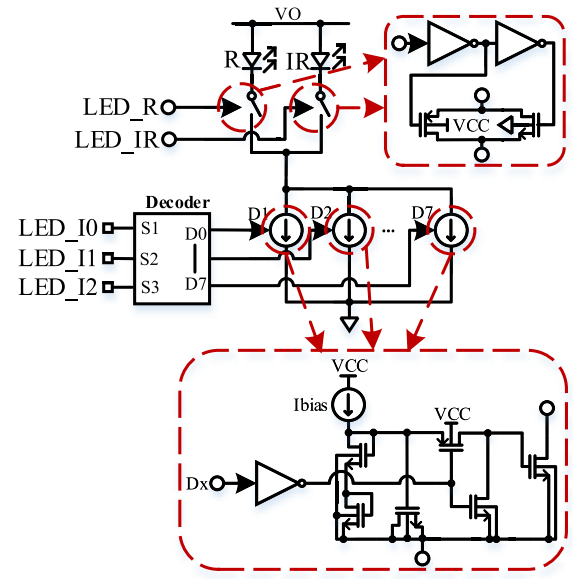

(a) LED driver

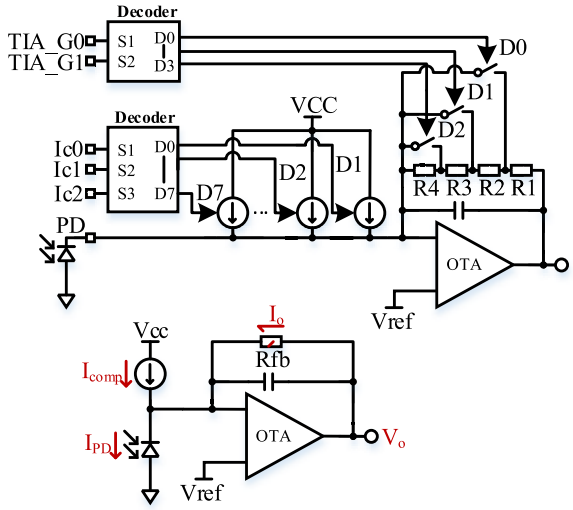

(b) TIA and current compensation

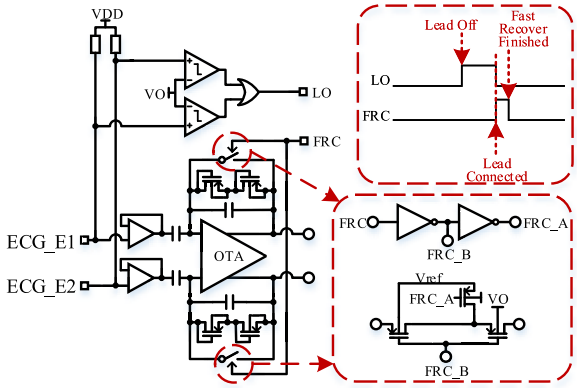

(c) ECG channel preamplifier

Fig. 4. Main AFE architecture.

components of blood but also ambient light [22]. This component limits the dynamic range of the PPG front-end input. Moreover, because ambient light drifts over time and changes with lighting conditions, statically compensating for this light becomes impossible [10]. In addition, the constant DC level occupies 96%–99% of the PPG signal and easily leads to saturation in the TIA. Therefore, we designed an auto-adjusted current compensation circuit. Three control bits (i.e., Ic0, Ic1, Ic2) are input into the decoder to control seven current sources with different currents (Table III). This circuit greatly reduces the DC level in the TIA output and significantly increases the gain of the TIA.

TABLE II
CONTROL BITS AND THE CORRESPONDING TIA TRANSRESISTANCE

Control bit	TIA transresistance (Ω)
00	200K
01	500K
10	1M
11	2M

TABLE III
CONTROL BITS OF THE TIA AND THE CORRESPONDING COMPENSATED CURRENT

Control bits	The compensated current of the TIA
000	0 μA
001	0.5 μA
010	1 μA
011	1.5 μA
100	2 μA
101	2.5 μA
110	3 μA
111	3.5 μA

3) Preamplifier of ECG Signal With Lead off Detection and Fast Recovery Function: In wearable applications, ECG electrodes tend to disconnect, and this causes an abnormal output for ECG channel. This necessitates the inclusion of lead-off detection. More and more papers applied capacitor coupled instrument amplifier as the first stage in ECG detection. The recovery time of capacitor coupled instrument amplifier has not been considered so far. This paper proposes a lead-off and fast recovery circuit for capacitor-coupled instrument amplifier in the preamplifier stage (Fig. 4(c)). When one of the electrodes (ECG_E1 or ECG_E2) disconnects, the output pin LO is at a high level because of the pull-up resistors and comparators. The output LO pin is connected to the MCU. During the lead-off period, the input of the OTA has a high voltage, whereas the output of the OTA remains abnormal. When the electrode connects again, the output LO recovers to a low level. Simultaneously, the OTA input recovers to the common mode voltage from the body, but the OTA output requires a long time to recover to the common mode voltage because of the long capacitor charge time. To ensure that the signal varies in real time, we designed a fast recovery circuit. After the LO signal becomes low, the MCU gives a high level signal to the FRC pin and makes the switches over the OTA turn on. The OTA output consequently becomes identical to the input, which is the common mode voltage. After the output recovers to the normal voltage, the switches turn off again. To avoid current leakage, a low-leakage switch structure is applied [23]. This circuit solves the recovery problem in capacitor coupled instrument amplifier without influencing the other performances.

B. Adaptive Adjustment Method

This work proposes an adaptive adjustment method that enables cooperation between the MCU and AFE IC, which allows the sensor to be adapted to any user and application.

1) ECG Channel: When the lead connection varies, the LO is changed. The rising or falling edge triggers MCU interruption. When the LO is high (lead off), the sampling of ECG is stopped. When LO is low (lead on), the fast recovery signal FRC is set to a high level for a short period. The sampling process starts. To ensure maximum amplitude for any user, the gain of the PGA is adjusted according to the detected ECG signal.

2) PPG Channel: First, the sensor detects the ambient TIA output V_{amb} when all the LEDs are turned off. According to this value, a compensation current is provided and dynamically adjusted until the ambient TIA output V_{amb} is equal or most close to the reference voltage $Vref$ at the positive input of TIA. The ambient current I_{amb} can be calculated from the present compensated current I_{comp_amb} as follows:

$$I_{amb} = (V_{amb} - Vref)/Rfb + I_{comp_amb}. \tag{1}$$

All the adjustable parameters for the subject are then calibrated when either the infrared or the red LED is turned on. Even when the ambient current is compensated for, the constant current I_{DC} due to the tissue and non-pulsatile components of blood occupies 96%–99% of the signal. Therefore, to maximize the AC amplitude of the PPG signal without saturation, both the ambient current I_{amb} and the constant current I_{DC} should be compensated for. However, the constant DC level (DC_R or DC_{IR}) of the PPG signal is used in SpO2 calculation. In addition, different users are expected to have varied thickness of fat and other tissue and thus the transmitted and reflected light may differ. To make the sensor usable for any user, the LED current and the gain of TIA requires calibration initially. Therefore, an individual adaptive adjustment method, to maximize the AC component of the PPG signal without saturation, and to detect the constant current I_{DC} for SpO2 calculation, is proposed.

As shown in Fig. 4(b), the PD current I_{PD}, when the infrared or red LED is turned on, is composed of

$$I_{PD} = I_{amb} + I_{DC} + I_{AC}, \tag{2}$$

where I_{AC} is the AC component due to the blood pulse. The LED current and transresistance Rfb are increased step by step, and the compensation current is adjusted to ensure that the output voltage V_o remains in the unsaturated range. The calibration is stopped until the maximum LED current and TIA gain are achieved. If there is a further increase, the output V_o is expected to be higher than the threshold, eventually leading to saturation. Then, the current on Rfb is calculated as

$$I_o = I_{PD} - I_{comp}, \tag{3}$$

and the output voltage is calculated as

$$\begin{aligned} V_o &= Vref + I_o \times Rfb \\ &= Vref + (I_{amb} + I_{DC} + I_{AC} - I_{comp}) \times Rfb. \end{aligned} \tag{4}$$

The constant DC level (DC_R or DC_{IR}) of the PPG signal can then be calculated from equation 4:

$$\begin{aligned} DC_{R/IR} &= I_{DC} \times Rfb \\ &= V_o - Vref - (I_{amb} - I_{comp}) \times Rfb, \end{aligned} \tag{5}$$

where the AC component $I_{AC} \times Rfb$ can be filtered by the low-pass filter. V_o is detected from the pin VO_LED, whereas I_{amb} is obtained from the first step. I_{comp} and Rfb are known based on the settings. The infrared and red PPG signals are then adjusted individually.

Through the application of the aforementioned method, the sensor can be used by any user with either a transmission or a reflection application.

III. HR, SpO2, and Blood Pressure Calculation Methods

The signals detected by the sensor can be used to calculate HR, SpO2, and blood pressure by using the methods introduced in the subsequent sections. With the methods introduced below, a real time monitoring software was designed to display the original signals and the calculated parameters.

A. HR and SpO2

The QRS waveforms are recognized from the ECG signal. HR is calculated using the R-R interval between the adjacent QRS waveforms.

The SpO2 is calibrated by the followed equation:

$$\begin{aligned} R &= (AC_R/DC_R)/(AC_{IR}/DC_{IR}), \\ SpO2 &= a \times R^2 + b \times R + c, \end{aligned} \tag{6}$$

Here, AC_R and AC_{IR} are the AC amplitudes of red and infrared PPG signals, respectively. Moreover, DC_R and DC_{IR} are the DC amplitudes of red and infrared PPG signals, respectively, and are calculated using the adaptive adjustment method introduced before. The coefficients (a, b, c) are calibrated by the vital sign simulator device (FLUKE ProSim 8) with an SpO2 of 80%–100%.

B. Continuous Blood Pressure

Pulse transit time (PTT) is an indicator of arterial blood pressure (BP) and has been widely used for cuffless BP measurement [24]. Additionally, studies have indicated that BP is associated with several static biometrics, such as age, gender, and body mass index (BMI) [25]–[27]. Inspired by these results, we developed a multi-parameter model based on PTT and static biometrics to evaluate the performance of the proposed sensor in estimating BP. The PTT is defined as the time interval between the R wave peak of ECG and the peak of PPG [20]. The static biometrics were age, gender, and body mass index (BMI). For each recording (a pair of synchronized ECG and PPG signals), PTT sequence was calculated from beat-to-beat signal and then averaged to obtain a global PTT. The multi-parameter takes as input a feature vector composed of global PTT, age, gender, and body mass index (BMI) and outputs the systolic BP (SBP) and diastolic BP (DBP) corresponding to each recording. As a pre-training process,

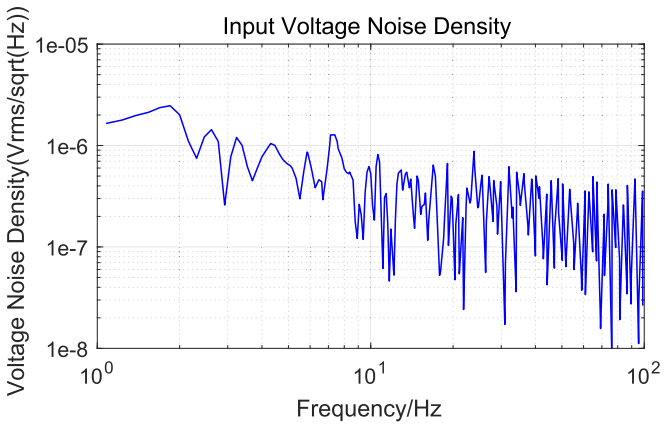

(a) Input referred noise of ECG channel

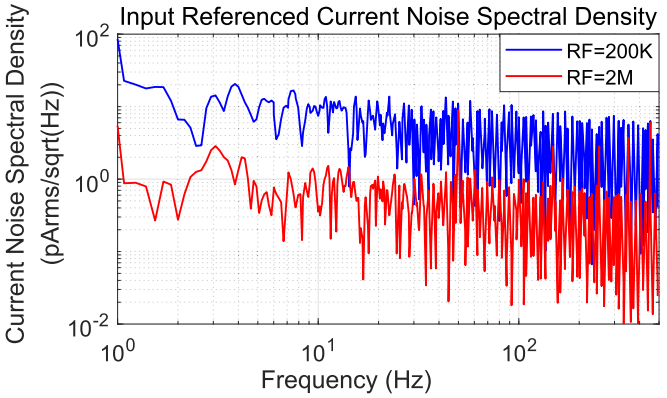

(b) Input referred noise of PPG channel with the transresistance of feedback resistor (RF)

Fig. 5. Measurement result of the gain bandwidth, CMRR and input referred noise of the ECG channel.

the support vector machine (SVM) algorithm was used to train the multi-parameter model on our pre-collected wearable dataset (164 volunteers, 17.68% male; PTT: 402.03 ± 30.42 ms; age: 57.66 ± 11.65 years; BMI: 23.83 ± 3.28 kg/m^2; DBP: 74.71 ± 10.6 mmHg; SBP: 114.65 ± 16.65 mmHg). The SVM algorithm is a popular machine learning tool for classification and regression and has been widely used in estimating BP [18], [28]. For an SVM regression problem, the goal is to find a function $f(x)$ for each training point x that deviates from targets y_n by a value no greater than ϵ, while being as flat as possible. This can be formulated as a convex optimization problem to minimize:

$$J(w) = 1/2\|w\|^2, subject\ to\ |y_i - (\langle w, x_i\rangle + b)| \leq \epsilon \quad (7)$$

where x_i is the feature vector (i.e., PTT and static biometrics), y_i is the target value of SBP or DBP, w is the weight vector, $\langle w, x_i\rangle + b$ is the estimation value for the feature vector x_i, and ϵ is a free parameter that serves as a threshold.

The Scikit-learn library in Python environment was employed for training an SVM regression model with "RBF kernel" for BP estimation. The hyper-parameters of the model, i.e., penalty C and kernel parameter γ, were optimized through grid searching.

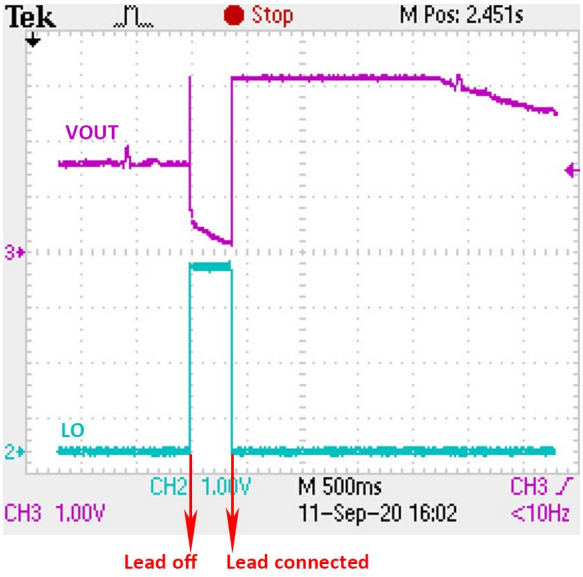

(a) The fast recover function is not enabled.

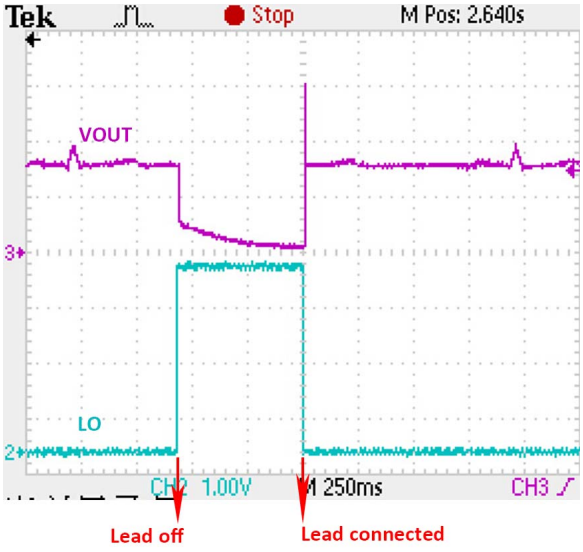

(b) The fast recover function is enabled.

Fig. 6. Measurement result of the lead off and fast recover function. LO is the output of the lead off instruction, while VOUT is the Output of ECG channel.

The trained model is applied in the monitoring software to calculated the BP in real time.

IV. Measurement Results

A. Measurement Results of AFE IC

The AFE was fabricated in CMOS 180 nm with the die size 1.27 × 1.27 mm^2. The whole chip consumed 170 μA of current under fully working. The bandwidth of the ECG channel was measured with a 1 μF external capacitor and different settings of the PGA. The result indicated a 54-60 dB gain and 0.5-100 Hz bandwidth. The common mode rejection ratio (CMRR) of the ECG channel was also measured by the positive and negative input pins connected together in the ECG channel. The result indicated that CMRR = 90 dB @50 Hz. The input referred noise of ECG channel was measured with

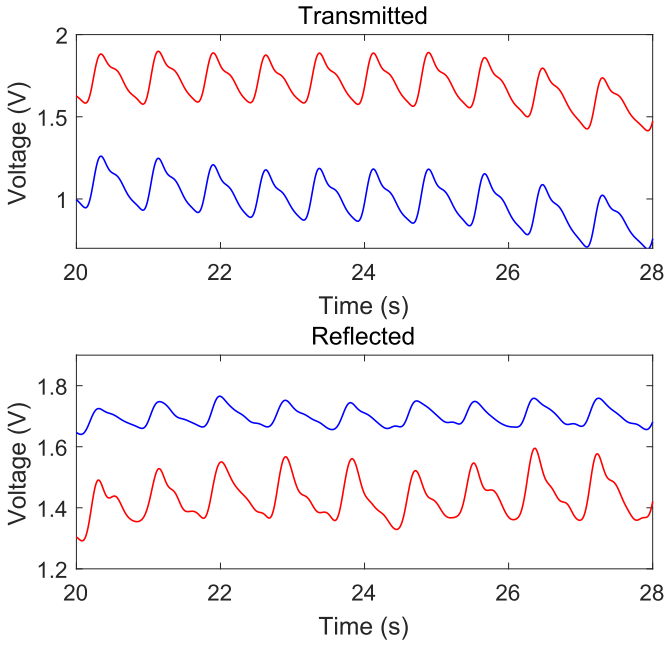

(a) The transmitted and reflected PPG signals.

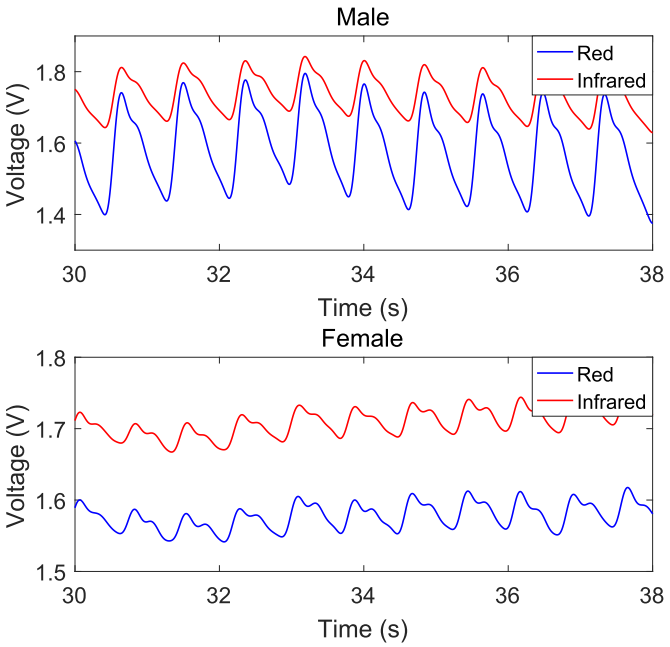

(b) The PPG signals for male and female subjects.

Fig. 7. Evaluation results of the adaptive adjust method.

a 60-dB gain. Fig. 5(a) presents the results with 4 μV in the 1-100 Hz bandwidth. Fig. 5(b) shows the TIA's input referred current noise density with various feedback resistor settings by the TIA gain control pins (TIA_G0 and TIA_G1). The current noise was inversely proportional to the transresistance of the feedback resistor (RF). For the transresistance between 200 KΩ and 2 MΩ, the input current noise at 10 Hz was from 0.4 pA/$\sqrt{Hz}$ with RF = 2 MΩ to 8 pA/$\sqrt{Hz}$ with RF = 200 KΩ.

Table IV compares our design with its recent state-of-the-art counterparts and the TI product AFE4900. The proposed

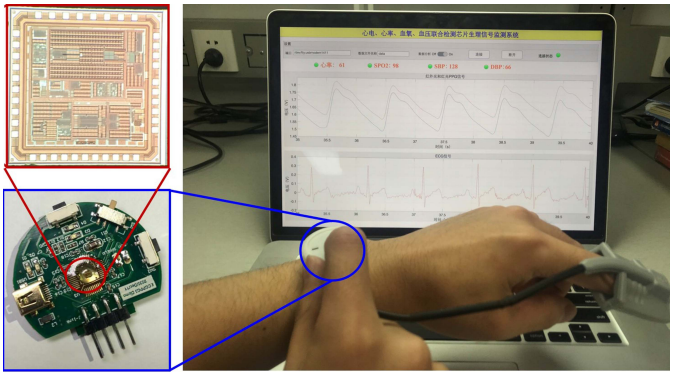

Fig. 8. The photos of the whole system.

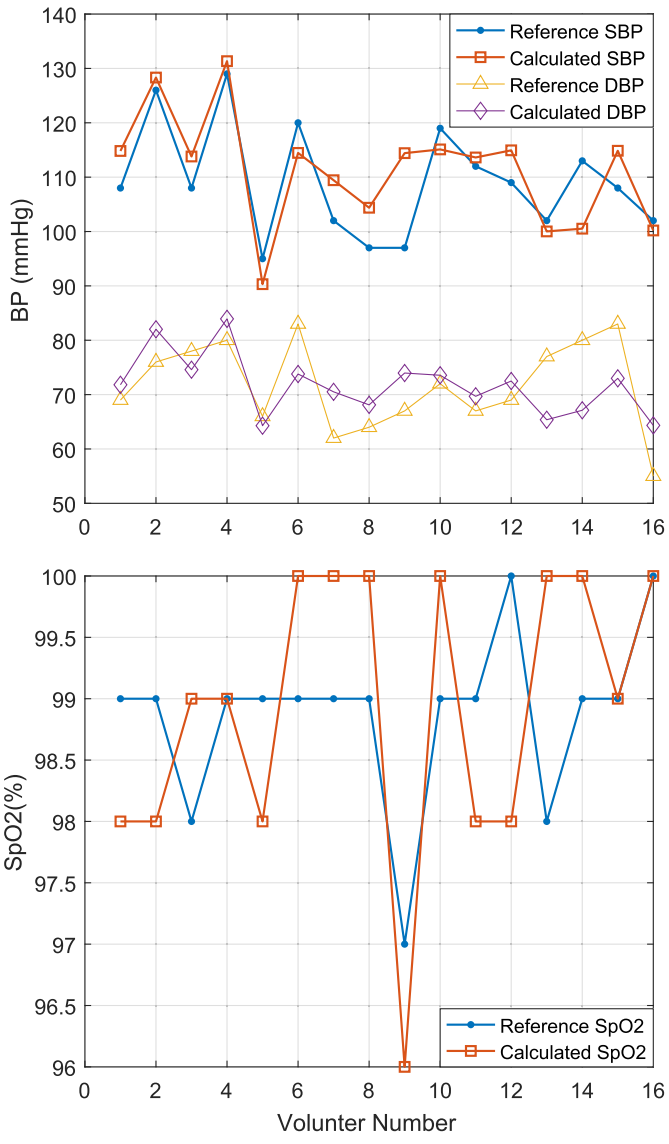

Fig. 9. The measurement resutl of the paramter accuracy.

IC performed comparably in current consumption, area, and PPG noise. In addition, our IC chip boasts comprehensive functions, such as adjustable gain, current compensation, lead off detection, and fast recovery—which are important for enabling widespread wearable application. The proposed

TABLE IV
PERFORMANCE COMPARISON

	This work	[29]	[30]	[11]	TI AFE4900	Richtek RT1025
Technology (nm)	180	180	130	55	-	-
Supply voltage (V)	3	1.2	1.2	1.2	1.8-1.9	2.8
Current consumption (μA)	170	53	43	305	627	780
Bandwidth (Hz)	0.5-100	200 (ECG)	0.5-70 (ECG)	0.5-150 (ECG) 0.1-20 (PPG)	-2k (ECG) 10-500 (PPG)	-28k/112k (ECG) -0.5k/1k/2k/4k (PPG)
CMRR (dB)	90@50 Hz	100	-	105	110	85
Input referred noise of ECG (μV_{rms})	4 (100 Hz BW)	0.8 (100 Hz BW)	1 (100 Hz BW)	0.733 (100 Hz BW)	2.5 (1-150 Hz BW)	1.69 (2k Hz BW)
Input referred noise of PPG (pA/$\sqrt{Hz}$ @ 10 Hz)	0.4 (RF=2 MΩ) 8 (RF=200 KΩ)	20 (RF=500 KΩ) 400 (RF=50 KΩ)	260 (100 Hz BW)	6 (RF=400 KΩ) 200 (RF=20 KΩ)	8 (RF=2 MΩ) 65 (RF=250 KΩ)	3.85 (RF=500KΩ) (0.1-5 Hz BW)
Gain of ECG (dB)	54-60 (adjustable)	40	25/52 (adjustable)	32/38/44	6.65-22.22	0-21.6
Gain of PPG (Ω)	200k-2M	20k	160k-3.5M	-	10k-2M	10k-1M
Current compensation for ambient	Yes	Yes	Yes	No	Yes	Yes
LED driver and current control	Yes, Yes	No	Yes, No	Yes	Yes	Yes
Lead off and fast recovery function	Yes	No	No	No	Yes	No
Area (mm^2)	1.27 × 1.27	1.1	7.5 × 7.5	18.49	2.6 × 2 (include package)	3.5×3.1 (include package)

IC was thus used in the subsequent experiment to build a multibiosensor for detecting various vital parameters.

B. Measurement Results of the Sensor

The sensor was implemented using the structure in Fig. 2. The sensor node detected the ECG and PPG signals and transmitted them to the PC with BLE. By using the proposed adaptive adjustment method introduced in Section 2.2, the fast recovery function was also tested. When the fast recovery function was not used, the output of the ECG channel required several seconds to recover to the normal level after the electrode was reconnected again (Fig. 6(a)). By using our proposed fast recovery function, the ECG channel output recovered to the normal signal in 1 ms (Fig. 6(b)). The source clock (CLK) was supplied by the MCU with 250 Hz frequency. Then the sampling frequency of ECG signal is 250 Hz, while PPG signal is 125Hz.

To evaluate the adaptive adjustment method in the PPG channel, transmitted and reflected PPG signals were detected. Similar to the many applications, such as those in smart watches (which can already detect reflected PPG signals), an AFE must be capable of detecting both transmitted and reflected PPG signals. However, a reflected PPG signal has a relatively weak AC amplitude and relatively high DC—which represents a challenge for the AFE. Herein, the aforementioned problem is resolved with the application of our adaptive adjustment method to the proposed AFE (Fig. 7(a)). Furthermore, for different users (e.g., male versus female) with different blood fusion and varied AC and DC behaviors in their PPG signals, our sensor can automatically adjust the LED current, TIA gain, and compensated current according to the current signals. The detected signals are shown in Fig. 7(b).

The photos for the whole sensor and the monitoring software are shown in Fig. 8. The PD and the red and infrared LEDs are integrated on the tips of the finger touching the sensor. The PD detects the light transmitted through the finger. Moreover, ECG electrodes are integrated on the sensor on the top and bottom sides. In this paper, a GUI was implemented with MATLAB to display the ECG and two-wavelength PPG signals. Moreover, four vital parameters were calculated from the signals in real time. All the parameters were updated every 2 s.

TABLE V
THE INFORMATION OF THE VOLUNTEERS

Gender	Age	Height	Weignt
Male (10) Female (6)	28.94±6.54	169.41±9.31	64.22±11.41

TABLE VI
THE MEAN ERROR AND STANDARD DEVIATION FOR SPO2, DBP AND SBP

Parameters	ME	STD
SpO2	0.94	0.56
DBP	0.04	7.34
SBP	2.10	7.07

The SpO2, DBP, and SBP were calculated in real time using the method introduced in the previous sections. After calibration, the SpO2 was calculated using the function in equation 6 with the coefficients $a = -30.41$, $b = -6.452$, and $c = 109.1$. The calibration curve was with $R^2 = 0.9995$ and $RMSE = 0.1461$. The DBP and SBP were calculated by the SVM model built before. The accuracy of SpO2, DBP, SBP were evaluated by 16 volunteers, as shown in Table V. The parameters calculated by the sensor system were compared with the measurement results from Mindray Monitor BeneVision M12. The results for every volunteers are shown in Fig. 9. The mean errors (ME) and Standard Deviations (STD) for SpO2, DBP and SBP are listed in Table VI.

The study was approved by the Institutional Review Board of the Shenzhen Institute of Advanced Technology, Chinese

Academy of Sciences, with approval number: SIAT-IRB-190215-H0287. Informed consent was obtained from all subjects before the experiment.

V. Conclusion

In this work, a wearable, multimodal, vital sign–monitoring sensor to monitor the four most crucial physiological parameters in patients with CVD—namely ECG, HR, SpO2, and continuous blood pressure—was constructed. In this sensor, the parameters are calculated from the ECG and two-wavelength PPG signals detected by an integrated AFE IC. The IC demonstrated excellent performance and satisfied the comprehensive requirements of practical applications. We also applied an adaptive adjustment method to automatically adjust the gain, LED current, and compensated current and to enable fast recovery after electrode reconnection. The sensor can thus be used for both transmission and reflection applications by a wide variety of users. Here, we tested the SpO2 algorithm in 16 volunteers with an error of 0.94% and evaluated the SBP and DBP with mean error $\pm$ standard deviation of -2.10 ± 7.07 mmHg and 0.04 ± 7.34 mmHg, respectively. The sensor provided excellent accuracy in signal detection and parameter calculation. In conclusion, our sensor is applicable for widespread applications among patients with CVD under home care.

References

[1] N. Wuthibenjaphonchai, M. Haruta, K. Sasagawa, T. Tokuda, S. Carrara, and J. Ohta, "Wearable and battery-free health-monitoring devices with optical power transfer," *IEEE Sensors J.*, vol. 21, no. 7, pp. 9402–9412, Apr. 2021.

[2] T. Liang and Y. J. Yuan, "Wearable medical monitoring systems based on wireless networks: A review," *IEEE Sensors J.*, vol. 16, no. 23, pp. 8186–8199, Dec. 2016.

[3] D. L. T. Wong *et al.*, "An integrated wearable wireless vital signs biosensor for continuous inpatient monitoring," *IEEE Sensors J.*, vol. 20, no. 1, pp. 448–462, Jan. 2020.

[4] J. I. Rodriguez-Labra, C. Kosik, D. Maddipatla, B. B. Narakathu, and M. Z. Atashbar, "Development of a PPG sensor array as a wearable device for monitoring cardiovascular metrics," *IEEE Sensors J.*, vol. 21, no. 23, pp. 26320–26327, Dec. 2021.

[5] H. Chen *et al.*, "Design of an integrated wearable multi-sensor platform based on flexible materials for neonatal monitoring," *IEEE Access*, vol. 8, pp. 23732–23747, 2020.

[6] S. Lee, B. Grundlehner, R. G. van der Westen, S. Polito, and C. Van Hoof, "Nightingale V2: Low-power compact-sized multi-sensor platform for wearable health monitoring," in *Proc. 41st Annu. Int. Conf. IEEE Eng. Med. Biol. Soc. (EMBC)*, Jul. 2019, pp. 1290–1293.

[7] Y. Zhang *et al.*, "Sleep stage classification using bidirectional LSTM in wearable multi-sensor systems," in *Proc. IEEE Conf. Comput. Commun. Workshops (INFOCOM WKSHPS)*, Apr. 2019, pp. 443–448.

[8] I. Kim, Y. A. Bhagat, J. Homer, and R. Lobo, "Multimodal analog front end for wearable bio-sensors," *IEEE Sensors J.*, vol. 16, no. 24, pp. 8784–8791, Dec. 2016.

[9] M. Konijnenburg *et al.*, "A multi(bio)sensor acquisition system with integrated processor, power management, 8×8 LED drivers, and simultaneously synchronized ECG, BIO-Z, GSR, and two PPG readouts," *IEEE J. Solid-State Circuits*, vol. 51, no. 11, pp. 2584–2595, Nov. 2016.

[10] J. Xu *et al.*, "A 36 μW 1.1 mm^2 reconfigurable analog front-end for cardiovascular and respiratory signals recording," *IEEE Trans. Biomed. Circuits Syst.*, vol. 12, no. 4, pp. 774–783, Aug. 2018.

[11] S. Song *et al.*, "A 769 μW battery-powered single-chip SoC with BLE for multi-modal vital sign monitoring health patches," *IEEE Trans. Biomed. Circuits Syst.*, vol. 13, no. 6, pp. 1506–1517, Dec. 2019.

[12] Y. Lee, H. Lee, S. Yoo, and H.-J. Yoo, "Sticker-type ECG/PPG concurrent monitoring system hybrid integration of CMOS SoC and organic sensor device," in *Proc. 38th Annu. Int. Conf. IEEE Eng. Med. Biol. Soc. (EMBC)*, Aug. 2016, pp. 2014–2017.

[13] A. Sharma *et al.*, "A sub-60 μA multimodal smart biosensing SoC with >80-dB SNR, 35-μA photoplethysmography signal chain," *IEEE J. Solid-State Circuits*, vol. 52, no. 4, pp. 1021–1033, Apr. 2017.

[14] I. Kim, P.-H. Lai, R. Lobo, and B. J. Gluckman, "Challenges in wearable personal health monitoring systems," in *Proc. 36th Annu. Int. Conf. IEEE Eng. Med. Biol. Soc.*, Aug. 2014, pp. 5264–5267.

[15] Y.-L. Zheng, B. P. Yan, Y.-T. Zhang, and C. C. Y. Poon, "An armband wearable device for overnight and cuff-less blood pressure measurement," *IEEE Trans. Biomed. Eng.*, vol. 61, no. 7, pp. 2179–2186, Jul. 2014.

[16] M. Kachuee, M. M. Kiani, H. Mohammadzade, and M. Shabany, "Cuff-less blood pressure estimation algorithms for continuous health-care monitoring," *IEEE Trans. Biomed. Eng.*, vol. 64, no. 4, pp. 859–869, Apr. 2017.

[17] Y.-Z. Yoon *et al.*, "Cuff-less blood pressure estimation using pulse waveform analysis and pulse arrival time," *IEEE J. Biomed. Health Informat.*, vol. 22, no. 4, pp. 1068–1074, Jul. 2018.

[18] F. Miao, N. Fu, Y.-T. Zhang, X.-R. Ding, X. Hong, and Q. Y. He, "A novel continuous blood pressure estimation approach based on data mining techniques," *IEEE J. Biomed. Health Informat.*, vol. 21, no. 6, pp. 1730–1740, Nov. 2017.

[19] F. Miao *et al.*, "Continuous blood pressure measurement from one-channel electrocardiogram signal using deep-learning techniques," *Artif. Intell. Med.*, vol. 108, Aug. 2020, Art. no. 101919.

[20] F. Miao, Z. Liu, J. Liu, B. Wen, Q. He, and Y. Li, "Multi-sensor fusion approach for cuff-less blood pressure measurement," *IEEE J. Biomed. Health Inform.*, vol. 24, no. 1, pp. 79–91, Jan. 2020.

[21] Y. Cheng and Y. Li, "A full custom fully integrated ECG measurement IC for healthcare applications," in *Proc. Int. Conf. Health Informat.*, Y.-T. Zhang, Ed. Cham, Switzerland: Springer, 2014, pp. 200–204.

[22] T. Tamura and Y. Maeda, *Photoplethysmogram*. Cham, Switzerland: Springer, 2018, pp. 159–192.

[23] Y. Wang, S. Doleschel, R. Wunderlich, and S. Heinen, "High energy efficient analog compressed sensing encoder for wireless ECG system," *Microelectron. J.*, vol. 56, pp. 10–16, Oct. 2016.

[24] X. Ding and Y.-T. Zhang, "Pulse transit time technique for cuffless unobtrusive blood pressure measurement: From theory to algorithm," *Biomed. Eng. Lett.*, vol. 9, no. 1, pp. 37–52, Feb. 2019.

[25] D. Wu, L. Xu, R. Zhang, H. Zhang, L. Ren, and Y.-T. Zhang, "Continuous cuff-less blood pressure estimation based on combined information using deep learning approach," *J. Med. Imag. Health Informat.*, vol. 8, no. 6, pp. 1290–1299, Aug. 2018.

[26] G. Barba *et al.*, "Gender-related differences in the relationships between blood pressure, age, and body size in prepubertal children," *Amer. J. Hypertension*, vol. 21, no. 9, pp. 1007–1010, Sep. 2008.

[27] S. R. Barnett *et al.*, "Effects of age and gender on autonomic control of blood pressure dynamics," *Hypertension*, vol. 33, no. 5, pp. 1195–1200, May 1999.

[28] Z. Liu, B. Zhou, Y. Li, M. Tang, and F. Miao, "Continuous blood pressure estimation from electrocardiogram and photoplethysmogram during arrhythmias," *Frontiers Physiol.*, vol. 11, pp. 1–13, Sep. 2020.

[29] J. Xu *et al.*, "A 665 μW silicon photomultiplier-based NIRS/EEG/EIT monitoring ASIC for wearable functional brain imaging," *IEEE Trans. Biomed. Circuits Syst.*, vol. 12, no. 6, pp. 1267–1277, Dec. 2018.

[30] J. Kim and H. Ko, "Reconfigurable multiparameter biosignal acquisition SoC for low power wearable platform," *Sensors*, vol. 16, no. 12, pp. 1–13, 2016.

Yishan Wang received the B.S. and M.S. degrees in biomedical engineering from Zhejiang University, China, in 2009 and 2012, respectively, and the Ph.D. degree from RWTH Aachen University, Germany.

She is currently an Associate Professor with the Shenzhen Institutes of Advanced Technology, Chinese Academy of Sciences. She is also presiding one National Natural Science Foundation of China and one Basic Research Foundation of Guangdong. Her research interests include wireless medical systems and integrated circuit design of analog front end for body sensors.

Fen Miao received the Ph.D. degree in computer science from the University of Chinese Academy of Sciences in 2015.

She is an Assistant Researcher with the Shenzhen Institutes of Advanced Technology, Chinese Academy of Sciences. She has published nearly 30 SCI/EI indexed papers in recent five years. She is also presiding one National Natural Science Foundation of China and one Basic Research Foundation of Shenzhen. Her research interests include health data analysis, cardiovascular disease modeling, and cuff-less blood pressure estimation.

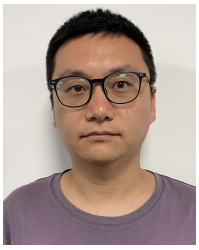

Qi An received the M.S. degree in microelectronics and solid state electronics from Fuzhou University, China, in 2014.

Currently, he is an Integrated Circuit Design Engineer at the Shenzhen Institutes of Advanced Technology, Chinese Academy of Science. His work focuses on body signal acquisition and processing ICs.

Zengding Liu received the master's degree in biomedical engineering from Chongqing University in 2017.

He is an Assistant Researcher with the Shenzhen Institutes of Advanced Technology, Chinese Academy of Science. His research interests include biomedical signal processing and cuff-less blood pressure modeling.

Cong Chen received the B.S. degree in measurement and control technology and instruments from Hangzhou Dianzi University, China, in 2017, and the M.S. degree in embedded systems from ISEN-Lille, France.

He is currently an Engineer with the Shenzhen Institutes of Advanced Technology, Chinese Academy of Science. His research interests include wearable medical devices and collaborative robot control systems and its electronic circuit.

Ye Li received the Ph.D. degree from Arizona State University in 2002.

He is currently a Professor with the Shenzhen Institutes of Advanced Technology, Chinese Academy of Sciences. He has applied for more than 90 related patents and software copyrights, more than 40 of which have been granted and many successfully achieved industrialization. He has published more than 120 SCI/EI indexed journals or international conference papers in the fields of mobile medical and health management and biomedical information technology in the last five years, more than 30 papers were indexed by SCI, and some were cited by journals of important influence, such as *Nature Review*. He has served as an organizing member/workshop Chairperson in important IEEE biomedical engineering related international conferences.